

Influence of the correlation prior on reconstruction of the dark energy equation of state

Yuhua Xu^{a,b} Hu Zhan^{b,c} and Yeuk-Kwan Edna Cheung^{a,d}

^aSchool of Physics, Nanjing University, 22 Hankou Road, Nanjing, Jiangsu 210093, China

^bCAS Key Laboratory of Space Astronomy and Technology, National Astronomical Observatories, Beijing 100101, China

^cKavli Institute for Astronomy and Astrophysics, Peking University, Beijing 100871, China

^dInstitute of Nuclear and Particle Physics, Demokritos National Research Centre, Athens, Greece

E-mail: yhxu@nao.cas.cn, zhanhu@nao.cas.cn, cheung@nju.edu.cn

Abstract. Non-parametric reconstruction of the dark energy equation of state (EoS) aims to determine the EoS as a function of redshift without invoking any particular dark energy model, so that the resulting EoS can be free of model-induced biases or artifacts. Without proper regularization, however, such reconstruction is often overwhelmed by the noise of poorly constrained modes. An intuitive regularization scheme is to assume a priori the dark energy EoS to evolve at most slowly with time, which may be enforced by a correlation between the EoS at different epochs. Indeed, studies that impose the correlation prior are able to significantly reduce the uncertainties of the reconstructed EoS and even show hints for dynamical dark energy.

In this work, we examine the correlation prior using mock datasets of type Ia supernovae (SNe Ia), baryonic acoustic oscillations (BAOs), age-derived Hubble parameter, Hubble constant, and cosmic microwave background. We find that even though the prior is designed to disfavor evolving equations of state, it can still accommodate spurious oscillating features at high significance. Within the 1000 mock datasets of existing observations that are generated for the concordance cosmological model, i.e., the input dark energy EoS $w = -1$, there are 688 (69) cases recovering an EoS that departs from -1 by more than 1σ (2σ) in one or more redshift bins. The reconstructed EoS turns up and down markedly in many cases. Moreover, inverting the signs of the randomly assigned errors of the mock data more or less reverses the behavior of the EoS. Spurious results occur even more frequently when idealized SN Ia and BAO data from future surveys are included. Our tests suggest that further studies are needed to ensure accurate reconstruction of the EoS with the correlation prior.

Keywords: cosmological parameters – dark energy – methods: data analysis

Contents

1	Introduction	1
2	Reconstructing the dark energy EoS	2
2.1	Non-parametric reconstruction with the correlation prior	2
2.2	Results of existing observations	4
3	Tests in the concordance cosmological model	5
3.1	Reconstruction using mock data of existing observations	6
3.1.1	Mock datasets	6
3.1.2	Examples of the reconstructed EoS	6
3.1.3	Statistics of the ensemble	8
3.2	Reconstruction using more data from future surveys	10
4	Summary	12
A	Fitting formulae for the CMB distance prior	12

1 Introduction

The discovery of accelerated cosmic expansion [1, 2] has inspired widespread efforts to determine its underlying physics (see, e.g., [3?–6] for reviews). One of the solutions proposed is to add a smooth component to the universe – dark energy in a broad sense – that drives the acceleration with its negative pressure. The equation of state (EoS), i.e., the ratio of pressure to density $w \equiv p/\rho$, is often used to characterize dark energy models. Since the EoS is inferred indirectly from geometry and growth measurements, one can define an effective dark energy EoS for theories that do not invoke dark energy at all. As such, the dark energy EoS can serve as a phenomenological discriminator for different theories of the accelerated cosmic expansion. It has indeed become a major task for next-stage dark energy surveys such as the Large Synoptic Survey Telescope¹ (LSST), *Euclid*², DESI³, and *WFIRST*⁴ to test various theories with accurate EoS measurements over a wide range of redshift.

Non-parametric reconstruction plays an important role in measuring the dark energy EoS [7, 8]. It tries to avoid potential biases or artifacts arising from specific model assumptions by adopting as little knowledge about the EoS as possible, though details of the implementation can still lead to different conclusions. For example, there are reports hinting at an evolving EoS and, hence, dynamical nature of dark energy [9–14], whereas others find consistency with the cosmological constant, i.e., $w = -1$ at all time [15–21]. The discrepancy calls for a closer examination of the reconstruction method.

In non-parametric reconstruction, the EoS is replaced by an approximation function that is constructed from its values $w_i \equiv w(a_i)$ at a series of scale factors a_i (or redshifts z_i). The approximation function is often chosen to be piece-wise constant or an interpolation of

¹<https://www.lsst.org/>.

²<http://sci.esa.int/euclid/>.

³<http://desi.lbl.gov/>.

⁴<http://wfirst.gsfc.nasa.gov/>.

$\{w_i\}$ [7, 18, 22–24]. The EoS values $\{w_i\}$ are then estimated from data and can vary freely to accommodate dark energy evolution to the extent the approximation function allows. In this way, one can be confident that the resulting EoS is completely determined by the data rather than some subtle effects of the particular dark energy model assumed in the first place. However, the drastically increased degrees of freedom also cause large uncertainties on the recovered EoS, making it less useful for testing dark energy models.

As pointed out in ref. [7], the uncertainties of the reconstructed EoS are dominated by poorly constrained eigenmodes, which typically oscillate more rapidly than well determined eigenmodes do. Since there is no strong case for a fast-oscillating EoS, it is reasonable to treat these poorly constrained modes as unphysical. One can thus reduce the EoS uncertainties by filtering out such eigenmodes in the result [7, 22], though the final EoS and its errors would depend on the number of eigenmodes being kept [11, 13]. Another way to reduce the EoS uncertainties is to regularize the reconstruction process with a correlation prior to suppress fast-varying modes in the posterior distribution of $\{w_i\}$ [25]. The correlation prior introduces an additional χ^2 term into the $\{w_i\}$ likelihood, which is derived from an assumed correlation function of the dark energy EoS at different epochs. Recent applications of this method have shown preference for dynamical dark energy over the cosmological constant at more than 3σ significance level [10].

Given the crucial role of the dark energy EoS in deciphering the accelerated cosmic expansion, one must ensure that the reconstruction method recovers the true EoS. While a thorough study of non-parametric reconstruction is needed, such an undertaking is well beyond the scope of this paper. Here we only test whether the correlation prior allows signatures of dynamical dark energy to be “reconstructed” from a universe dominated by the cosmological constant and cold dark matter (the Λ CDM model). For convenience, we refer to the cosmological model that allows w to vary in time as the \tilde{w} CDM model.

The rest of the paper is organized as follows. Section 2 describes the method of non-parametric reconstruction of the dark energy EoS with the correlation prior and reproduces the result in ref. [10]. In section 3, we test the correlation prior using mock datasets of current observations and future surveys that are generated for the Λ CDM universe. Section 4 summarizes the results and concludes the paper.

2 Reconstructing the dark energy EoS

2.1 Non-parametric reconstruction with the correlation prior

Non-parametric reconstruction of the dark energy EoS is essentially estimating a discrete set of EoS values $\{w_i\}$ that are used to interpolate the EoS as a function of time (or its equivalent). The value of w_i at each interpolation node is allowed to vary freely to accommodate arbitrary evolution of dark energy. Piece-wise constant interpolation and linear interpolation are common choices for approximating the EoS [7, 18, 22–24]. We find no significant difference between the results of the two schemes as long as there are enough interpolation nodes to cover the range of the scale factor of all the data.

Following refs. [9, 10, 25], we adopt the piece-wise constant approximation. The scale factor interval $[a_{\min}, 1]$ is evenly divided into N bins of width $\Delta a = (1 - a_{\min})/N$ with each bin assigned a w_i . The choice of a_{\min} is determined by the scale factor of the highest-redshift data point excluding the cosmic microwave background (CMB). The distance to the last scattering surface, as derived from the CMB, is the only data point that contains dark

energy information at $a < a_{\min}$. Therefore, we assign a single EoS parameter to the interval $[a_{\text{CMB}}, a_{\min}]$.

With the observables expressed in terms of $\{w_i\}$ and other parameters, one can use Markov Chain Monte Carlo (MCMC) sampling to map the posterior distribution

$$\mathcal{P}(\boldsymbol{\theta}|\mathbf{d}) \propto P(\boldsymbol{\theta}) \mathcal{L}(\mathbf{d}|\boldsymbol{\theta}), \quad (2.1)$$

where $\boldsymbol{\theta}$ is the full set of parameters including $\{w_i\}$, \mathbf{d} is the data vector, $P(\boldsymbol{\theta})$ is the prior, and $\mathcal{L}(\mathbf{d}|\boldsymbol{\theta})$ is the likelihood of \mathbf{d} given $\boldsymbol{\theta}$. The likelihood function is approximated as a multivariate Gaussian $\mathcal{L}(\mathbf{d}|\boldsymbol{\theta}) \propto \exp(-\frac{1}{2}\chi_{\text{data}}^2)$ with

$$\chi_{\text{data}}^2 = (\mathbf{d} - \mathbf{d}^{\text{th}})^T \mathbf{C}_d^{-1} (\mathbf{d} - \mathbf{d}^{\text{th}}), \quad (2.2)$$

where \mathbf{d}^{th} is the data vector calculated theoretically from $\boldsymbol{\theta}$, and \mathbf{C}_d is the covariance matrix of the data. Note that \mathbf{C}_d may depend on $\boldsymbol{\theta}$.

To reduce the uncertainties and enforce the smoothness of the reconstructed EoS, ref. [25] proposes to apply a prior $P(\mathbf{w}) \propto \exp(-\frac{1}{2}\chi_{\text{prior}}^2)$ with

$$\chi_{\text{prior}}^2 = [(\mathbf{I} - \mathbf{S})\mathbf{w}]^T \mathbf{C}_w^{-1} [(\mathbf{I} - \mathbf{S})\mathbf{w}], \quad (2.3)$$

where $\mathbf{w} \equiv \{w_i\}$, \mathbf{I} is the identity matrix, \mathbf{S} is the smoothing matrix, and \mathbf{C}_w is the covariance matrix of \mathbf{w} . The total χ^2 for the MCMC sampling is then $\chi_{\text{tot}}^2 = \chi_{\text{data}}^2 + \chi_{\text{prior}}^2$. The covariance matrix \mathbf{C}_w is derived from an assumed correlation function of the dark energy EoS:

$$C_{w,ij} = \frac{1}{(\Delta a)^2} \int_{a_i}^{a_i+\Delta a} da \int_{a_j}^{a_j+\Delta a} da' \xi_w(|a - a'|), \quad (2.4)$$

$$\xi_w(|a - a'|) \simeq \frac{\sigma_w^2}{\pi a_c} \frac{1 - a_{\min}}{1 + (|a - a'|/a_c)^2}, \quad (2.5)$$

where σ_w^2 is the variance of the mean value of $w(a)$ within the interval $[a_{\min}, 1]$, and a_c is the correlation length. The smoothing matrix \mathbf{S} performs a local average of \mathbf{w} , i.e.,

$$S_{ij} = \begin{cases} 1/N_i & |a_i - a_j| \leq a_c \\ 0 & \text{else} \end{cases}, \quad (2.6)$$

with N_i being the number of the EoS bins in the range $[a_i - a_c, a_i + a_c]$. We adopt the same “weak prior” ($\sigma_w = 0.04$ and $a_c = 0.06$) used in refs. [9, 10] throughout this paper.

The χ^2 contribution of the correlation prior, i.e., eq. (2.3), can be rewritten more concisely as $\chi_{\text{prior}}^2 = \mathbf{w}^T \mathbf{F}_w \mathbf{w}$ with $\mathbf{F}_w = (\mathbf{I} - \mathbf{S})^T \mathbf{C}_w^{-1} (\mathbf{I} - \mathbf{S})$. Projecting \mathbf{w} onto the complete set of eigenmodes of \mathbf{F}_w , one obtains

$$\chi_{\text{prior}}^2 = \sum_{i=1}^N \lambda_i (\mathbf{w}^T \mathbf{e}_i)^2, \quad (2.7)$$

where \mathbf{e}_i is the i -th eigenmode of \mathbf{F}_w , and λ_i is its corresponding eigenvalue. Figure 1 gives an example of the eigenspectrum of the correlation prior. The eigenmodes are ordered by the number of zero-crossing nodes: the higher the mode number, the more the eigenmode oscillates. The eigenvalue increases quickly with the mode number, penalizing fast-varying modes through eq. (2.7). As expected, the χ^2 contribution of the correlation prior vanishes for the constant EoS.

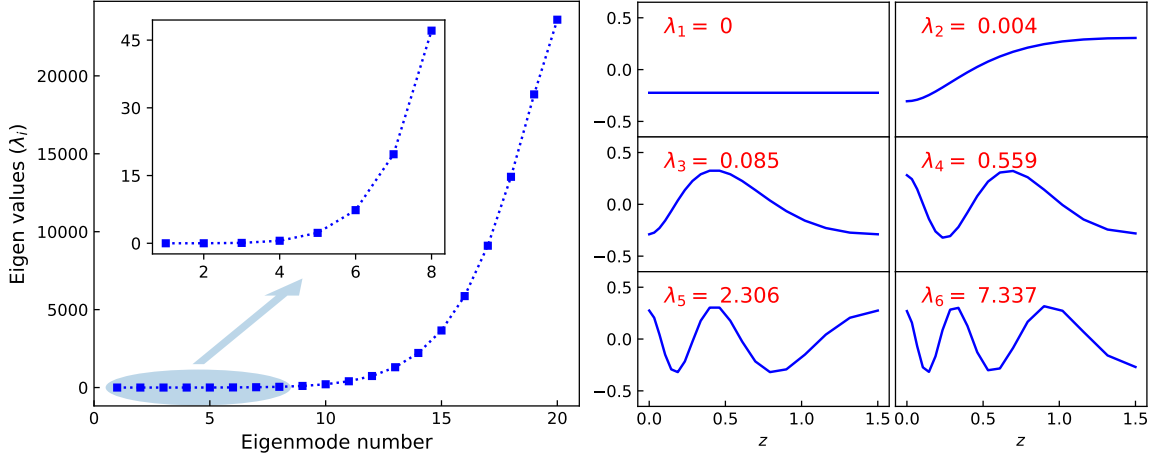


Figure 1. *Left panel:* Eigenspectrum of the correlation prior with $\sigma_{\bar{w}} = 0.04$, $a_c = 0.06$, $N = 20$ and $a_{\min} = 0.4$. The eigenmodes are ordered by the number of zero-crossing nodes. The inset is a zoom-in of the first 8 modes. *Right panel:* The first six eigenmodes in redshift coordinate.

2.2 Results of existing observations

We implement a cosmological parameter estimation program *ClassMC*⁵ to reconstruct the dark energy EoS, which incorporates the Boltzmann code *CLASS* [26, 27, v2.5.0] (modified to allow the dark energy EoS to evolve arbitrarily) and the affine-invariant ensemble sampler [28] *IMCMC*⁶ [29]. The sampled chains are analyzed using *GetDist*⁷. For simplicity, we assume a flat geometry and ignore dark energy clustering [30, 31], which are not expected to alter the conclusion of this study.

We use the following observations to reconstruct the dark energy EoS: *Planck* CMB temperature and polarization power spectra⁸ [32, 33, *Planck*-2015], SDSS-II/SNLS3 type Ia supernova (SN Ia) joint light-curve analysis data [34, 35, JLA], BOSS DR12 baryon acoustic oscillation (BAO) measurements of the angular diameter distance $D_A(z)$ and the Hubble parameter $H(z)$ in combination with the comoving sound horizon at the drag epoch r_d [36, 37], the Hubble parameter $H(z)$ derived from galaxy ages [38, OHD], the Hubble constant $H_0 = 73.24 \pm 1.74 \text{ km s}^{-1} \text{ Mpc}^{-1}$ [39], BAO $D_A(z)$ and $H(z)$ measurements from the Ly α forest [40], as well as BAO $D_V(z)$ measurements from the 6dF galaxy survey [41] and the SDSS DR7 Main Galaxy Sample [42]. This dataset includes all the data of the ALL16 combination in ref. [10] except the WiggleZ galaxy power spectra [43] and the CFHTLenS weak-lensing shear power spectra [44], which do not have a significant impact on the reconstructed EoS. The data of CMB, SN Ia, BAO, OHD, H_0 , and Ly α forest are assumed to be mutually independent, so that the total covariance matrix \mathbf{C}_d has a block-diagonal form with one block for each type of observation. Moreover, to keep the computational cost manageable, we replace the CMB power spectra with the CMB distance prior [45] for the ensemble study in section 3, and, hence, a consistency check between the results of the two types of CMB data is performed in this section. We refer to the joint dataset with the CMB power spectra as JD16 and that with the CMB distance prior as JD16*.

⁵<https://github.com/xyh-cosmo/ClassMC>.

⁶<https://github.com/xyh-cosmo/imcmc>.

⁷<https://github.com/cmbant/getdist>.

⁸Likelihood products: plik_lite.v18.TTTEEE.clk and lowl.SMW_70_dx11d.2014.10.03.v5c_Ap.clk.

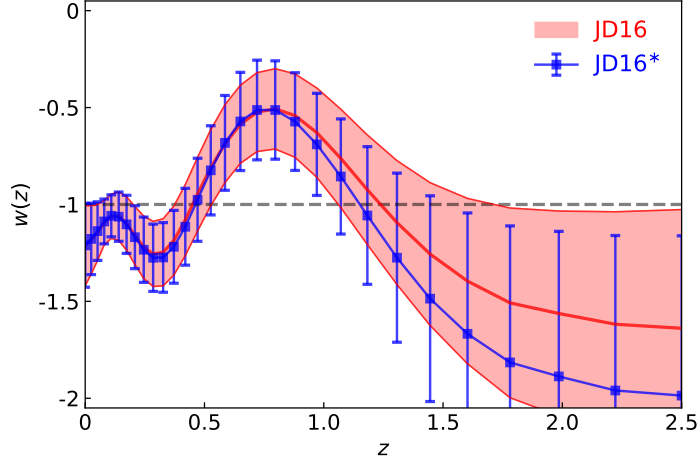


Figure 2. Dark energy EoS reconstructed from JD16 (red band) and JD16* (blue squares). The band and error bars indicate the marginalized 1σ error.

The set of parameters to be estimated is

$$\theta \equiv \{H_0, \Omega_b, \Omega_c, A_s, n_s, \tau, w_0, \dots, w_{29}, \mathcal{N}\}, \quad (2.8)$$

where Ω_b is the baryon density parameter, Ω_c is the cold dark matter density parameter, A_s and n_s are, respectively, the amplitude and the spectral index of the primordial density power spectrum, τ is the optical depth due to reionization, and \mathcal{N} includes all the nuisance parameters. For SNe Ia, the nuisance parameters are the B-band absolute magnitude M_B , the magnitude offset Δ_M for more massive host galaxies, and the light-curve parameters α and β [35]; for *Planck*, the nuisance parameter is A_{Planck} , the absolute map calibration [46, 47]. The EoS parameters $\{w_i\}$ are assigned according to the scheme described in section 2.1 with $a_{\min} = 0.286$ ($z_{\max} = 2.5$). Since the parameters A_s , n_s , τ , and A_{Planck} do not affect the CMB distance prior, they are removed from the parameter set when JD16* is used for reconstruction.

The results of reconstruction are shown in figure 2. The dark energy EoS from JD16* (blue squares) traces that from JD16 (red band) very well, and they display marked resemblance to those in refs. [10, 13]. Figure 2 demonstrates that the CMB distance prior, which greatly reduces the amount of computation, can replace the full CMB power spectra for non-parametric reconstruction of the dark energy EoS.

3 Tests in the concordance cosmological model

As with any parameter estimation problem, one must ensure the fidelity of the reconstructed dark energy EoS. Specifically, the actual EoS should be the only source of any statistically significant feature in the reconstructed EoS. This section performs tests on mock data generated for the flat Λ CDM universe to see whether characteristics of dynamical dark energy can appear in the reconstructed EoS at high significance. These tests are included in the ClassMC package as examples.

3.1 Reconstruction using mock data of existing observations

3.1.1 Mock datasets

The JD16* dataset is used as a template to simulate an ensemble of 1000 mock datasets for the Λ CDM model (Λ JD16* datasets). Details are as follows.

- The fiducial cosmology is specified by the *Planck* 2018 base- Λ CDM cosmological parameters [48, table 1]. In particular, $H_0 = 67.32 \text{ km s}^{-1} \text{ Mpc}^{-1}$, $\Omega_b h^2 = 0.022383$, and $\Omega_c h^2 = 0.12011$, where h is the reduced Hubble constant.
- The covariance matrix of Λ JD16* is the same as that of JD16*, except that the light-curve model parameters α and β in the JLA covariance matrix are fixed to their best-fit values [34, 35].
- The redshift of each data point is exactly the same as that in JD16*. The fiducial values of the distance, the Hubble constant, and the Hubble parameter are given by the fiducial cosmology. Random errors are drawn from the multivariate Gaussian distribution as defined by the covariance matrix of Λ JD16* and then added to these fiducial values to form a realization of Λ JD16*.
- The covariance matrix of Λ JD16* is factorized into $\mathbf{C}_d = \mathbf{Q} \mathbf{D} \mathbf{Q}^{-1}$ with \mathbf{Q} being an orthogonal matrix and \mathbf{D} being a diagonal matrix. A random vector \mathbf{v} is constructed by drawing each element v_i from a zero-mean Gaussian distribution of variance D_{ii} . The transformation $\Delta \mathbf{d} = \mathbf{Q} \mathbf{v}$ generates the random errors that follow the multivariate Gaussian distribution as defined by \mathbf{C}_d . These errors are then added to the fiducial values to form a realization of Λ JD16*.
- For the SN Ia sample, the B-band absolute magnitude M_B assumes the fiducial value of -19.3 , and the magnitude offset Δ_M is set to zero.
- The fiducial values of the quantities constituting the CMB distance prior are calculated using the fitting formulae from refs. [49, 50] (see appendix A).

Altogether, there are 758 degrees of freedom for estimating the set of parameters $\{H_0, \Omega_b, \Omega_c, w_0, \dots, w_{29}, M_B\}$ from each Λ JD16* dataset. For convenience, we refer to the aforementioned multivariate Gaussian distribution of the data as $\mathcal{G}(\mathbf{C}_d)$.

3.1.2 Examples of the reconstructed EoS

An example of the reconstructed dark energy EoS is shown in the left panel of figure 3 (red band). The corresponding scaled mock distance and Hubble parameter data of JLA SNe Ia, BOSS DR12 BAO, OHD, and Ly α forest BAO are displayed in the right panel of figure 3, along with the values calculated using the best-fit \tilde{w} CDM model (red solid lines). The difference between the best-fit $\chi^2_{\text{data,BF}}$ and that of the Λ CDM model $\chi^2_{\text{data},\Lambda}$ is $\Delta\chi^2_{\text{data}} = -7.07$ and would have been interpreted as a 2.7σ ($|\Delta\chi^2_{\text{data}}|^{1/2}$) preference for the \tilde{w} CDM model over the Λ CDM model [10]. Although χ^2_{data} does not include the contribution from the prior directly, the difference $\Delta\chi^2_{\text{data}}$ is affected by the prior through the selection of the best-fit model.

The correlation prior is an integral part of the parameter estimation process that produces the reconstructed EoS. It is also appropriate to take the prior contribution into account and compare the goodness-of-fit between the two models based on χ^2_{tot} . The resulting

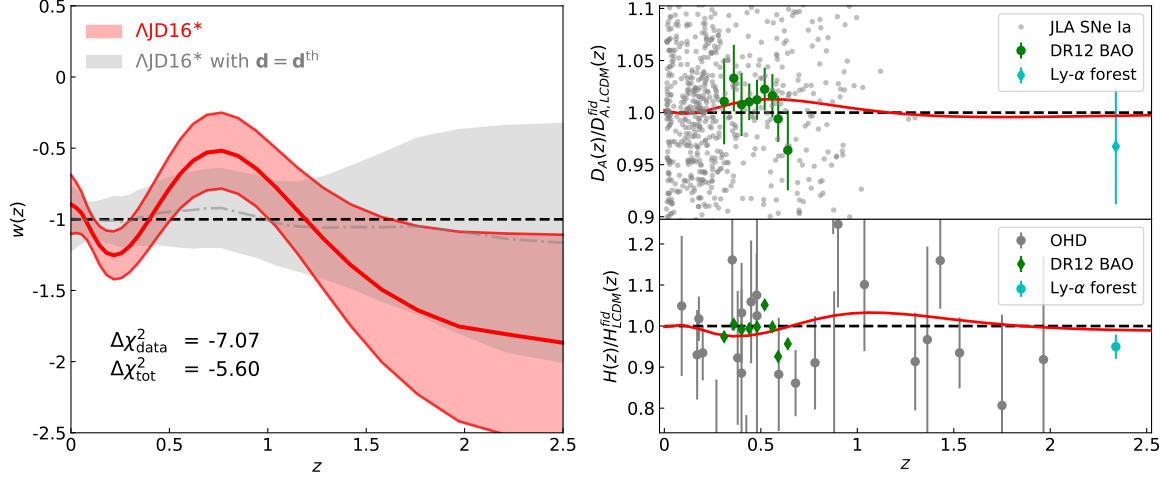


Figure 3. *Left panel:* Dark energy EoS (red band) reconstructed from a realization of Λ JD16*. The grey band is the result with all the data set exactly by the fiducial Λ CDM model. *Right panel:* Mock data of the angular diameter distance and the Hubble parameter scaled by corresponding values of the fiducial Λ CDM model. For SNe Ia, the angular diameter distances are converted from their luminosity distances and the uncertainties are omitted for clarity. The red solid lines are the predictions of the best-fit \tilde{w} CDM model.

$\Delta\chi_{\text{tot}}^2 = -5.60$ is weaker than $\Delta\chi_{\text{data}}^2$ as it should be, and the preference for the \tilde{w} CDM model becomes less significant. This particular example is selected for its resemblance to the result in ref. [10]. It suggests that the usual statistical interpretation of $\Delta\chi_{\text{data}}^2$ (or even $\Delta\chi_{\text{tot}}^2$) may not be sufficient as evidence for dynamical dark energy from non-parametric reconstruction of the EoS with the correlation prior.

Since the correlation prior is designed to suppress fast-varying EoS modes not to create any modes, the survived oscillating feature must be sourced in the mock data. The underlying Λ CDM cosmology of Λ JD16* does not produce the signal either. This leaves the statistical errors of the data the only suspect. The grey band in the left panel of figure 3 is the result of a test in which all the mock data are set to their fiducial values, i.e., $\mathbf{d} = \mathbf{d}^{\text{th}}$. In this way, the fiducial Λ CDM model is the best-fit with $\chi_{\text{tot}}^2 = 0$ by construction, and the result is highly consistent with $w = -1$ as expected. It is evident from this test that the errors in the data are the source of the oscillating feature in the EoS reconstructed from the Λ JD16* dataset.

Figure 4 displays nine randomly selected examples of the reconstructed EoS (red bands). In seven of the nine examples, the recovered EoS deviates from the fiducial model $w = -1$ by more than 1σ at least once over the whole redshift range. Because of the overall constraint from the distance to the last scattering surface, it is unlikely for the recovered dark energy EoS to always stay above or below $w = -1$. Therefore, a departure of the EoS in one bin from $w = -1$ often causes the EoS in other bin(s) to deviate in the opposite direction for compensation, producing a wiggle in the EoS.

For each Λ JD16* dataset in figure 4, we also create a conjugate dataset by inverting the signs of the errors of the data in the original dataset. The fiducial Λ CDM model has exactly the same χ_{tot}^2 with both datasets. Interestingly, the original and conjugate results are roughly symmetric around $w = -1$ at $z \lesssim 1$, which demonstrates that the signature of dynamical dark energy in the EoS reconstructed from Λ JD16* indeed originates from the

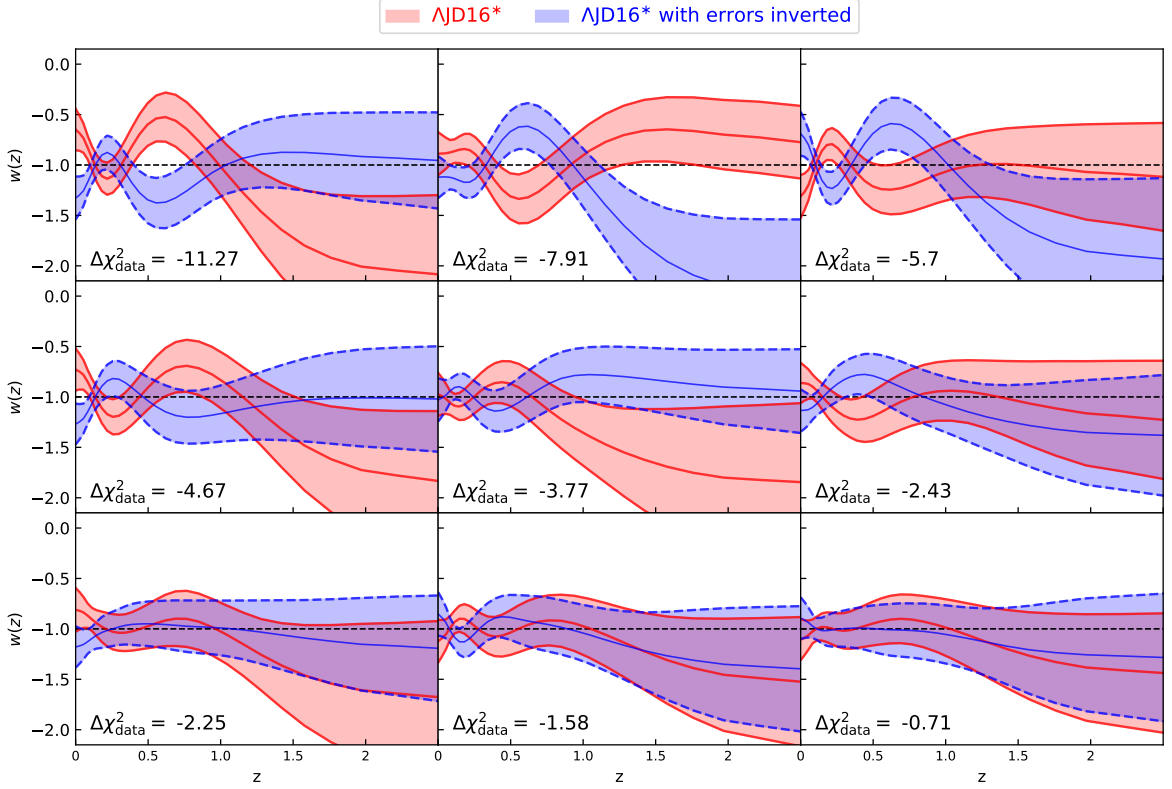


Figure 4. Randomly selected examples of the dark energy EoS reconstructed from Λ JD16* datasets. The red bands are the original results, and the blue bands are those with all the random errors of the data inverted. The panels are ordered by $\Delta\chi^2_{\text{data}}$ of the original results.

random errors of the data.

3.1.3 Statistics of the ensemble

Figure 5 examines the reconstructed dark energy EoS in terms of the distributions of the best-fit χ^2_{tot} , $\Delta\chi^2_{\text{data}}$ with respect to the Λ CDM model, and p -value of the Kolmogorov-Smirnov test (KS test) for each Λ JD16* dataset. The p -value provides an estimate of the probability of the data following a particular distribution. Although the mock datasets are drawn from the multivariate Gaussian distribution $\mathcal{G}(\mathbf{C}_d)$, there is a finite probability for some datasets to appear incompatible with $\mathcal{G}(\mathbf{C}_d)$ at high significance and produce low p -values. Therefore, we take the p -value as a measure of apparent departure from $\mathcal{G}(\mathbf{C}_d)$ and check if it is related to the occurrence of artificial EoS features.

In practice, we rotate and rescale the error vector $\Delta\tilde{\mathbf{d}} = \mathbf{C}_d^{-1/2}(\mathbf{d} - \mathbf{d}^{\text{th}})$, so that the resulting elements $\Delta\tilde{d}_i$ all follow the unit-variance Gaussian distribution. The KS test is then performed on the set of $\Delta\tilde{d}_i$ of each mock dataset against the unit-variance Gaussian distribution. The results are displayed intuitively in three groups according to the behavior of the best-fit EoS: (1) the weak-wiggle group, which has an EoS always less than 1σ away from $w = -1$, i.e., $|1 + w_i| < \sigma_{w_i}$ in all bins; (2) the moderate-wiggle group, which has $|1 + w_i| \geq \sigma_{w_i}$ in at least one bin and $|1 + w_i| < 2\sigma_{w_i}$ in all bins; and (3) the strong-wiggle group, which has $|1 + w_i| \geq 2\sigma_{w_i}$ in at least one bin.

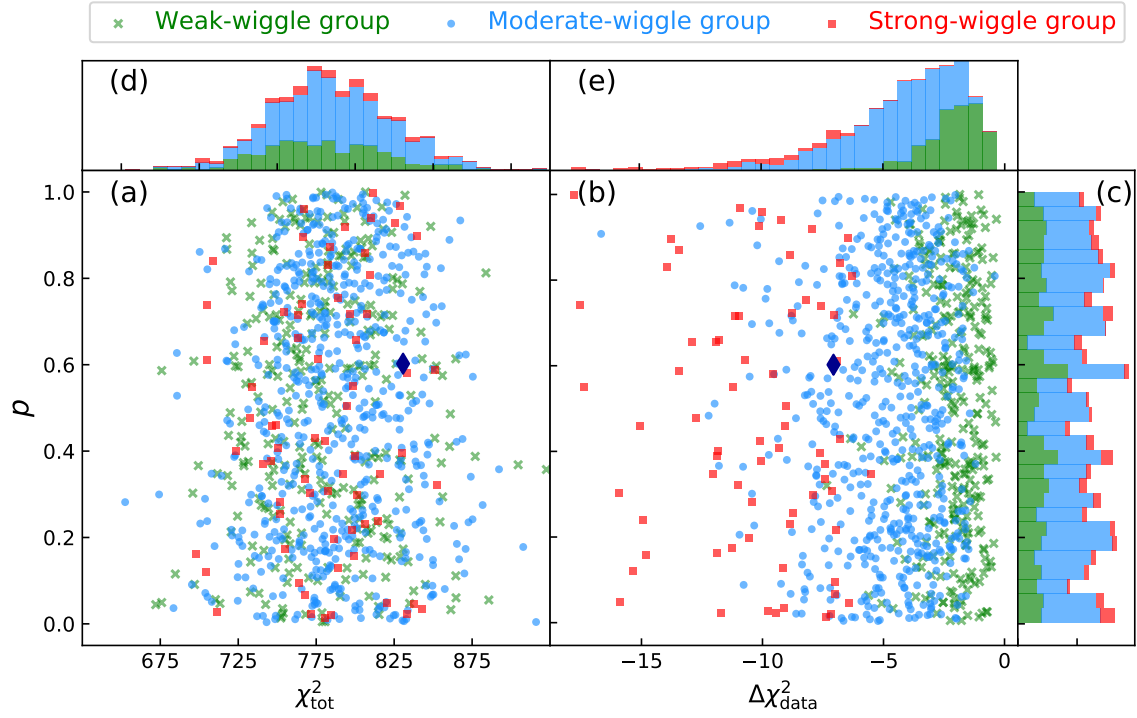


Figure 5. Distributions of the best-fit χ^2_{tot} , $\Delta\chi^2_{\text{data}}$, and p -values of the 1000 Λ JD16* datasets. *Panels (a) and (b):* Green crosses, blue dots, and red squares represent, respectively, the weak-wiggle group, the moderate-wiggle group, and the strong-wiggle group. See text for definitions of the three groups. The blue diamond corresponds to the Λ JD16* result in figure 3, which belongs to the moderate-wiggle group. The color-coding is the same for the other panels. *Panel (c):* Stacked histogram of the KS-test p -values of the mock datasets. *Panels (d) and (e):* Stacked histograms of the best-fit χ^2_{tot} and $\Delta\chi^2_{\text{data}}$.

It is seen from panels (a) and (b) of figure 5 that the p -value is uncorrelated with the best-fit χ^2_{tot} and $\Delta\chi^2_{\text{data}}$. Highly significant spurious signals of dynamical dark energy (large $|\Delta\chi^2_{\text{data}}|$) can be obtained from Λ JD16* datasets over the full range of p -values from appearing incompatible with $\mathcal{G}(\mathcal{C}_d)$ (p -value ~ 0) to a perfect match (p -value ~ 1). The example EoS in figure 3 as marked by a blue diamond in figure 5 is not an extreme case in terms of p -value, χ^2_{tot} , and $\Delta\chi^2_{\text{data}}$. The histogram of the p -value in panel (c) is roughly flat as expected. Moreover, none of the p -value histogram components of the three EoS groups displays any clear trend with the p -value itself.

Histograms of χ^2_{tot} and $\Delta\chi^2_{\text{data}}$ are shown, respectively, in panels (d) and (e) of figure 5. The χ^2_{tot} distribution peaks around 775 with a maximum χ^2_{tot} of 923.6, which is normal for parameter estimation with 758 degrees of freedom. The three EoS groups behave similarly in the χ^2_{tot} histogram but do differ in the $\Delta\chi^2_{\text{data}}$ histogram in a way that is consistent with their intuitive classification: the weak-wiggle group (312 cases out of 1000 realizations) generally does not give a strong preference for dynamical dark energy, i.e., mostly $|\Delta\chi^2_{\text{data}}| < 5$, and dominates the whole distribution at $|\Delta\chi^2_{\text{data}}| \lesssim 2.5$; the strong-wiggle group (69 cases) has $|\Delta\chi^2_{\text{data}}| > 5$ and is the main contributor at $|\Delta\chi^2_{\text{data}}| \gtrsim 9$; and the moderate-wiggle group (619 cases) is an intermediate between the other two groups. Of the 1000 mock datasets, there are 72 cases preferring the \tilde{w} CDM model to the Λ CDM model at $\geq 3\sigma$ level ($|\Delta\chi^2_{\text{data}}| \geq 9$).

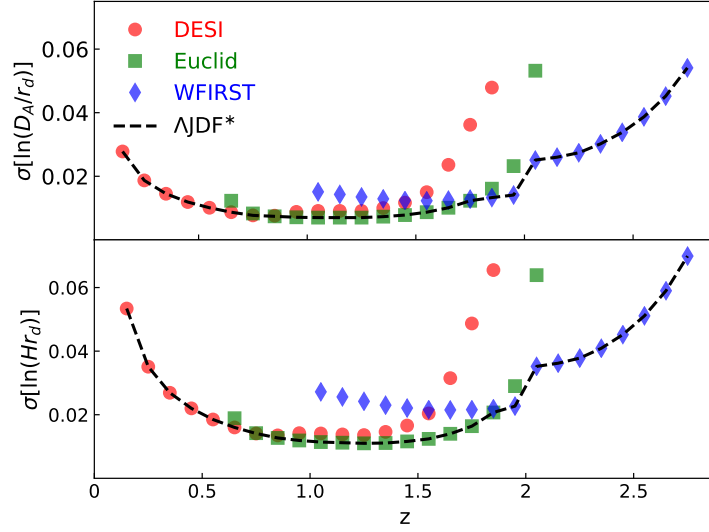


Figure 6. *Upper panel:* Expected fractional errors of the angular diameter distance $D_A(z)$ from future BAO surveys [51]. The lower envelope of the distance errors is used for Λ JDF* datasets. *Lower panel:* Same as the upper panel but for the Hubble parameter $H(z)$.

3.2 Reconstruction using more data from future surveys

It is often assumed that the effect of the prior weakens as more data becomes available. Indeed, upcoming surveys, such as LSST, DESI, *Euclid* and *WFIRST*, will provide unprecedentedly powerful data for dark energy studies. Hence, we test here whether future data could help eliminate artificial EoS features.

Using the Λ JD16* data model of the existing observations as a baseline, we add the expected *WFIRST* SN Ia sample and replace the original mock BAO data with those anticipated from DESI, *Euclid*, and *WFIRST* to form the future Λ JDF* data model. For each Λ JDF* dataset, mock data of future BAO and SN Ia observations are generated randomly according to the following description.

- The expected errors of the angular diameter distance $D_A(z)$ and the Hubble parameter $H(z)$ from DESI, *Euclid*, and *WFIRST* are given by ref. [51] and are shown in figure 6. For simplicity, we do not attempt to combine all the BAO data in a statistically consistent way, which would involve properly treating overlapping volumes and overlapping samples between the surveys as well as correlations between the BAO data. Instead, we keep only the data point of the smallest error at each redshift and neglect correlations between the BAO data.
- The redshift distribution and error model of the *WFIRST* SNe Ia data are adopted from ref. [52]. There is a total of 2725 SNe Ia in the redshift range $0.1 < z < 1.7$. The errors of the distance modulus are assumed to be independent between different SNe Ia and follow a redshift-dependent Gaussian distribution with a total variance

$$\sigma_\mu^2 = \sigma_{\text{int}}^2 + \sigma_{\text{meas}}^2 + \sigma_{\text{lens}}^2 + \sigma_{\text{sys}}^2, \quad (3.1)$$

where $\sigma_{\text{int}} = 0.09$ is the intrinsic spread of the SN Ia peak absolute magnitude (after correction for the light-curve shape and spectral properties), $\sigma_{\text{meas}} = 0.08$ is the photome-

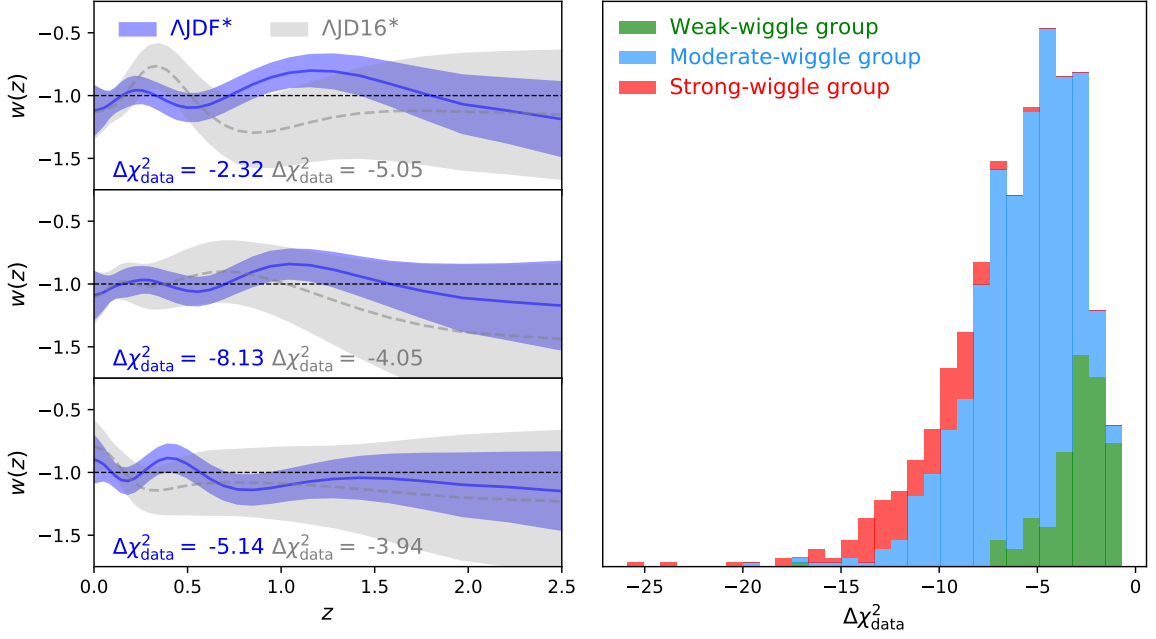


Figure 7. Results of dark energy EoS reconstruction from the Λ JDF* datasets. *Left panel:* Three randomly selected examples of the reconstructed EoS (blue) along with their corresponding Λ JD16* results (grey). *Right panel:* Stacked histogram of the best-fit $\Delta\chi^2_{\text{data}}$. The color-coding is the same as that in figure 5.

try error, $\sigma_{\text{lens}} = 0.07z$ accounts for lensing magnification, and $\sigma_{\text{sys}} = 0.02/(1+z)/1.8$ is attributed to potential systematics.

The parameters to be estimated from each Λ JDF* dataset are the same as those in section 3.1, and there are 3515 degrees of freedom in total. One may worry that ignoring the correlations between the data can lead to unduly tight constraints on the EoS. Since we only need to check the significance of spurious features in the EoS that is reconstructed with more data, ignoring the correlations does not affect the result qualitatively.

The left panel of figure 7 displays three randomly selected examples of the reconstructed dark energy EoS from Λ JDF* datasets (blue bands) along with the ones from corresponding Λ JD16* datasets (grey bands). The reduction of the uncertainties of the reconstructed EoS with future SNe Ia and BAO data is quite notable. However, the preference for dynamical dark energy, as quantified by $\Delta\chi^2_{\text{data}}$, can become even stronger for some Λ JDF* datasets. In fact, the $\Delta\chi^2_{\text{data}}$ histogram of the Λ JDF* results in figure 7 is shifted towards more negative values with respect to that of the Λ JD16* results in figure 5. On average, the Λ JDF* datasets increase $|\Delta\chi^2_{\text{data}}|$ by 1.72 over that of the Λ JD16* datasets. The occurrence of the moderate-wiggle group and the strong-wiggle group is also increased, respectively, from 619 cases and 69 cases to 724 cases and 100 cases out of 1000 realizations. There are now 171 cases reaching $|\Delta\chi^2_{\text{data}}| \geq 9$, more than doubling those of the Λ JD16* results. Hence, there is no guarantee that non-parametric reconstruction of the dark energy EoS with the correlation prior can eliminate spurious EoS features with more data.

4 Summary

We have carried out a number of tests on non-parametric reconstruction of the dark energy EoS with the correlation prior as proposed by refs. [25]. While we obtain an oscillating EoS similar to that in ref. [10] using largely the same set of observational data, highly resemblant results can also be obtained from Λ JD16* mock datasets of existing observations that are generated under the flat Λ CDM model. The Λ JDF* mocks that include future SN Ia and BAO data reduce the EoS uncertainties considerably, though they actually increase the occurrence of significant spurious features in the reconstructed EoS. For instance, the fraction of realizations that prefers dynamical dark energy to the cosmological constant at $\geq 3\sigma$ level is 7.2% with the Λ JD16* mocks and is boosted to 17.1% with the Λ JDF* mocks. It is evident that, with the correlation prior, adding more data does not necessarily recover the true EoS.

Figure 4 demonstrates that the source of the oscillating EoS features can be traced to random errors in the data. However, random errors always exist and can produce all sorts of modes in the EoS. Once the poorly determined high-frequency EoS modes are suppressed by the correlation prior, the EoS uncertainties become small enough to give a good chance for the surviving slowly-oscillating modes to stand out at high significance. In other words, even though those poorly determined high-frequency EoS modes are undesirable, they are part of the complete statistical description of the reconstructed EoS without which one would severely underestimate the uncertainties of the EoS.

Since random errors in the data can generate time-varying EoS modes that behave like dynamical dark energy, it would be difficult to draw a conclusion based on existing results. As such, more studies of the correlation prior and reconstruction method are needed to accurately determine the dark energy EoS and test it against theoretical models.

Acknowledgments

HZ acknowledges support from the National Science Foundation of China grant No. 11721303, the National Key R&D Program of China grant No. 2016YFB1000605, and China Manned Space Program through the Space Application System. This research of YKEC has been supported in parts by the NSF China under Contract No. 11775110, and No. 11690034. YKEC also acknowledges the European Union’s Horizon 2020 research and innovation programme (RISE) under the Marie Skłodowska-Curie grant agreement No. 644121, and the Priority Academic Program Development for Jiangsu Higher Education Institutions (PAPD).

A Fitting formulae for the CMB distance prior

The CMB distance prior consists of the acoustic scale l_A , the shift parameter R , and the photon decoupling redshift z_* . These quantities are calculated using the fitting formulae from refs. [49, 50]:

$$l_A = (1 + z_*) \frac{\pi D_A(z_*)}{r_s(z_*)}, \quad (\text{A.1})$$

$$R = \frac{\sqrt{(\Omega_b + \Omega_c)H_0^2}}{c} (1 + z_*) D_A(z_*), \quad (\text{A.2})$$

$$z_* = 1048 \left[1 + 0.00124(\Omega_b h^2) \right]^{-0.738} \left[1 + g_1(\Omega_b h^2 + \Omega_c h^2)^{g_2} \right], \quad (\text{A.3})$$

where

$$g_1 = \frac{0.0783(\Omega_b h^2)^{-0.238}}{1 + 39.5(\Omega_b h^2)^{0.763}}, \quad (\text{A.4})$$

$$g_2 = \frac{0.560}{1 + 21.1(\Omega_b h^2)^{1.81}}. \quad (\text{A.5})$$

The angular diameter distance $D_A(z)$ and the sound horizon $r_s(z)$ are defined as:

$$D_A(z) = \frac{c}{(1+z)} \int_0^z \frac{dz'}{H(z')}, \quad (\text{A.6})$$

$$r_s(z) = \frac{c}{\sqrt{3}} \int_0^{(1+z)^{-1}} \frac{da}{a^2 H(a) \sqrt{1 + (3\Omega_b/4\Omega_\gamma)a}}, \quad (\text{A.7})$$

where Ω_γ is the radiation density parameter.

References

- [1] A. G. Riess, A. V. Filippenko, P. Challis, A. Clocchiatti, A. Diercks, P. M. Garnavich et al., *Observational Evidence from Supernovae for an Accelerating Universe and a Cosmological Constant*, *Astron. J.* **116** (Sept., 1998) 1009–1038, [[astro-ph/9805201](#)].
- [2] S. Perlmutter, G. Aldering, G. Goldhaber, R. A. Knop, P. Nugent, P. G. Castro et al., *Measurements of Ω and Λ from 42 High-Redshift Supernovae*, *Astrophys. J.* **517** (June, 1999) 565–586, [[astro-ph/9812133](#)].
- [3] J. A. Frieman, M. S. Turner and D. Huterer, *Dark Energy and the Accelerating Universe*, *Ann. Rev. Astron. & Astrophys.* **46** (Sept., 2008) 385–432, [[0803.0982](#)].
- [4] R. R. Caldwell and M. Kamionkowski, *The Physics of Cosmic Acceleration*, *Annual Review of Nuclear and Particle Science* **59** (Nov., 2009) 397–429, [[0903.0866](#)].
- [5] M. Li, X.-D. Li, S. Wang and Y. Wang, *Dark Energy*, *Communications in Theoretical Physics* **56** (Sept., 2011) 525–604, [[1103.5870](#)].
- [6] D. H. Weinberg, M. J. Mortonson, D. J. Eisenstein, C. Hirata, A. G. Riess and E. Rozo, *Observational probes of cosmic acceleration*, *Phys. Rep.* **530** (Sept., 2013) 87–255, [[1201.2434](#)].
- [7] D. Huterer and G. Starkman, *Parametrization of Dark-Energy Properties: A Principal-Component Approach*, *Physical Review Letters* **90** (Jan., 2003) 031301, [[astro-ph/0207517](#)].
- [8] V. Sahni and A. Starobinsky, *Reconstructing Dark Energy*, *International Journal of Modern Physics D* **15** (2006) 2105–2132, [[astro-ph/0610026](#)].
- [9] G.-B. Zhao, R. G. Crittenden, L. Pogosian and X. Zhang, *Examining the evidence for dynamical dark energy*, *Phys. Rev. Lett.* **109** (Oct, 2012) 171301.
- [10] G.-B. Zhao, M. Raveri, L. Pogosian, Y. Wang, R. G. Crittenden, W. J. Handley et al., *Dynamical dark energy in light of the latest observations*, *Nature Astronomy* **1** (Sept., 2017) 627–632, [[1701.08165](#)].
- [11] W. Zheng and H. Li, *Constraints on parameterized dark energy properties from new observations with principal component analysis*, *Astroparticle Physics* **86** (Jan, 2017) 1–10.
- [12] Y. Wang, L. Pogosian, G.-B. Zhao and A. Zucca, *Evolution of Dark Energy Reconstructed from the Latest Observations*, *Astrophys. J. Lett.* **869** (Dec., 2018) L8, [[1807.03772](#)].
- [13] J.-P. Dai, Y. Yang and J.-Q. Xia, *Reconstruction of the Dark Energy Equation of State from the Latest Observations*, *Astrophys. J.* **857** (Apr., 2018) 9.

- [14] Z. Zhang, G. Gu, X. Wang, Y.-H. Li, C. G. Sabiu, H. Park et al., *Non-parametric dark energy reconstruction using the tomographic Alcock-Paczynski test*, *arXiv e-prints* (Feb, 2019) arXiv:1902.09794, [[1902.09794](#)].
- [15] P. Serra, A. Cooray, D. E. Holz, A. Melchiorri, S. Pandolfi and D. Sarkar, *No evidence for dark energy dynamics from a global analysis of cosmological data*, *Phys. Rev. D* **80** (Dec., 2009) [121302](#), [[0908.3186](#)].
- [16] T. Holsclaw, U. Alam, B. Sansó, H. Lee, K. Heitmann, S. Habib et al., *Nonparametric dark energy reconstruction from supernova data*, *Phys. Rev. Lett.* **105** (Dec, 2010) [241302](#).
- [17] N. Said, C. Baccigalupi, M. Martinelli, A. Melchiorri and A. Silvestri, *New constraints on the dark energy equation of state*, *Phys. Rev. D* **88** (Aug, 2013) [043515](#), [[1303.4353](#)].
- [18] F. Y. Wang and Z. G. Dai, *Estimating the uncorrelated dark energy evolution in the Planck era*, *Phys. Rev. D* **89** (Jan., 2014) [023004](#), [[1312.4613](#)].
- [19] Planck Collaboration, P. A. R. Ade, N. Aghanim, M. Arnaud, M. Ashdown, J. Aumont et al., *Planck 2015 results. XIV. Dark energy and modified gravity*, *Astron. & Astrophys.* **594** (Sept., 2016) [A14](#), [[1502.01590](#)].
- [20] S. Hee, J. A. Vázquez, W. J. Handley, M. P. Hobson and A. N. Lasenby, *Constraining the dark energy equation of state using Bayes theorem and the Kullback-Leibler divergence*, *Mon. Not. Roy. Astron. Soc.* **466** (Apr, 2017) [369–377](#), [[1607.00270](#)].
- [21] W. J. M. Ribeiro, *Observational Constraints on the Dark Energy Equation of State*, *arXiv e-prints* (Apr, 2019) arXiv:1904.11068, [[1904.11068](#)].
- [22] D. Huterer and A. Cooray, *Uncorrelated estimates of dark energy evolution*, *Phys. Rev. D* **71** (Jan., 2005) [023506](#), [[astro-ph/0404062](#)].
- [23] R. G. Crittenden, L. Pogosian and G.-B. Zhao, *Investigating dark energy experiments with principal components*, *J. Cosmo. Astropart. Phys.* **12** (Dec., 2009) [025](#), [[astro-ph/0510293](#)].
- [24] J. A. Vázquez, M. Bridges, M. P. Hobson and A. N. Lasenby, *Reconstruction of the dark energy equation of state*, *Journal of Cosmology and Astro-Particle Physics* **2012** (Sept., 2012) [020](#), [[1205.0847](#)].
- [25] R. G. Crittenden, G.-B. Zhao, L. Pogosian, L. Samushia and X. Zhang, *Fables of reconstruction: controlling bias in the dark energy equation of state*, *J. Cosmo. Astropart. Phys.* **2** (Feb., 2012) [048](#), [[1112.1693](#)].
- [26] J. Lesgourgues, *The cosmic linear anisotropy solving system (class) i: Overview*, *ArXiv e-prints* (Apr., 2011) , [[1104.2932](#)].
- [27] D. Blas, J. Lesgourgues and T. Tram, *The cosmic linear anisotropy solving system (class). part ii: Approximation schemes*, *J. Cosmo. Astropart. Phys.* **7** (July, 2011) [034](#), [[1104.2933](#)].
- [28] J. Goodman and J. Weare, *Ensemble samplers with affine invariance*, *Communications in Applied Mathematics and Computational Science, Vol. 5, No. 1, p. 65-80, 2010* **5** (2010) [65–80](#).
- [29] Y. Xu, H. Zhan and Y.-K. E. Cheung, *Reconstructing the cosmic expansion history with a monotonicity prior*, *Journal of Cosmology and Astro-Particle Physics* **2018** (Mar., 2018) [045](#), [[1710.02947](#)].
- [30] G.-B. Zhao, J.-Q. Xia, M. Li, B. Feng and X. Zhang, *Perturbations of the quintom models of dark energy and the effects on observations*, *Phys. Rev. D* **72** (Dec, 2005) [123515](#), [[astro-ph/0507482](#)].
- [31] M. Li, Y. Cai, H. Li, R. Brandenberger and X. Zhang, *Dark energy perturbations revisited*, *Physics Letters B* **702** (Aug, 2011) [5–11](#), [[1008.1684](#)].

- [32] Planck Collaboration, R. Adam, P. A. R. Ade, N. Aghanim, Y. Akrami, M. I. R. Alves et al., *Planck 2015 results. I. Overview of products and scientific results*, *Astron. & Astrophys.* **594** (Sept., 2016) A1, [[1502.01582](#)].
- [33] Planck Collaboration, N. Aghanim, M. Arnaud, M. Ashdown, J. Aumont, C. Baccigalupi et al., *Planck 2015 results. XI. CMB power spectra, likelihoods, and robustness of parameters*, *Astron. & Astrophys.* **594** (Sept., 2016) A11, [[1507.02704](#)].
- [34] M. Betoule, J. Marriner, N. Regnault, J.-C. Cuillandre, P. Astier, J. Guy et al., *Improved photometric calibration of the SNLS and the SDSS supernova surveys*, *Astron. & Astrophys.* **552** (Apr., 2013) A124, [[1212.4864](#)].
- [35] M. Betoule, R. Kessler, J. Guy, J. Mosher, D. Hardin, R. Biswas et al., *Improved cosmological constraints from a joint analysis of the SDSS-II and SNLS supernova samples*, *Astron. & Astrophys.* **568** (Aug., 2014) A22, [[1401.4064](#)].
- [36] G.-B. Zhao, Y. Wang, S. Saito, D. Wang, A. J. Ross, F. Beutler et al., *The clustering of galaxies in the completed SDSS-III Baryon Oscillation Spectroscopic Survey: tomographic BAO analysis of DR12 combined sample in Fourier space*, *Mon. Not. Roy. Astron. Soc.* **466** (Apr., 2017) 762–779, [[1607.03153](#)].
- [37] Y. Wang, G.-B. Zhao, C.-H. Chuang, A. J. Ross, W. J. Percival, H. Gil-Marín et al., *The clustering of galaxies in the completed SDSS-III Baryon Oscillation Spectroscopic Survey: tomographic BAO analysis of DR12 combined sample in configuration space*, *Mon. Not. Roy. Astron. Soc.* **469** (Aug, 2017) 3762–3774, [[1607.03154](#)].
- [38] M. Moresco, L. Pozzetti, A. Cimatti, R. Jimenez, C. Maraston, L. Verde et al., *A 6% measurement of the Hubble parameter at $z \sim 0.45$: direct evidence of the epoch of cosmic re-acceleration*, *J. Cosmo. Astropart. Phys.* **5** (May, 2016) 014, [[1601.01701](#)].
- [39] A. G. Riess, L. M. Macri, S. L. Hoffmann, D. Scolnic, S. Casertano, A. V. Filippenko et al., *A 2.4% Determination of the Local Value of the Hubble Constant*, *Astrophys. J.* **826** (July, 2016) 56, [[1604.01424](#)].
- [40] T. Delubac, J. E. Bautista, N. G. Busca, J. Rich, D. Kirkby, S. Bailey et al., *Baryon acoustic oscillations in the Ly α forest of BOSS DR11 quasars*, *Astron. & Astrophys.* **574** (Feb., 2015) A59, [[1404.1801](#)].
- [41] F. Beutler, C. Blake, M. Colless, D. H. Jones, L. Staveley-Smith, L. Campbell et al., *The 6dF Galaxy Survey: baryon acoustic oscillations and the local Hubble constant*, *Mon. Not. Roy. Astron. Soc.* **416** (Oct, 2011) 3017–3032, [[1106.3366](#)].
- [42] A. J. Ross, L. Samushia, C. Howlett, W. J. Percival, A. Burden and M. Manera, *The clustering of the SDSS DR7 main Galaxy sample - I. A 4 per cent distance measure at $z = 0.15$* , *Mon. Not. Roy. Astron. Soc.* **449** (May, 2015) 835–847, [[1409.3242](#)].
- [43] D. Parkinson, S. Riemer-Sørensen, C. Blake, G. B. Poole, T. M. Davis, S. Brough et al., *The WiggleZ Dark Energy Survey: Final data release and cosmological results*, *Phys. Rev. D* **86** (Nov., 2012) 103518, [[1210.2130](#)].
- [44] C. Heymans, E. Grocutt, A. Heavens, M. Kilbinger, T. D. Kitching, F. Simpson et al., *CFHTLenS tomographic weak lensing cosmological parameter constraints: Mitigating the impact of intrinsic galaxy alignments*, *Mon. Not. Roy. Astron. Soc.* **432** (July, 2013) 2433–2453, [[1303.1808](#)].
- [45] Q.-G. Huang, K. Wang and S. Wang, *Distance priors from Planck 2015 data*, *J. Cosmo. Astropart. Phys.* **12** (Dec., 2015) 022, [[1509.00969](#)].
- [46] Planck Collaboration, P. A. R. Ade, N. Aghanim, M. Arnaud, M. Ashdown, J. Aumont et al., *Planck 2015 results. XIII. Cosmological parameters*, *Astron. & Astrophys.* **594** (Sept., 2016) A13, [[1502.01589](#)].

- [47] Planck Collaboration, R. Adam, P. A. R. Ade, N. Aghanim, M. Arnaud, M. Ashdown et al., *Planck 2015 results. VIII. High Frequency Instrument data processing: Calibration and maps*, *Astron. & Astrophys.* **594** (Sep, 2016) A8, [[1502.01587](#)].
- [48] Planck Collaboration, N. Aghanim, Y. Akrami, M. Ashdown, J. Aumont, C. Baccigalupi et al., *Planck 2018 results. VI. Cosmological parameters*, *arXiv e-prints* (July, 2018) , [[1807.06209](#)].
- [49] Y. Wang and P. Mukherjee, *Observational constraints on dark energy and cosmic curvature*, *Phys. Rev. D* **76** (Nov., 2007) 103533, [[astro-ph/0703780](#)].
- [50] E. Komatsu, J. Dunkley, M. R. Nolta, C. L. Bennett, B. Gold, G. Hinshaw et al., *Five-Year Wilkinson Microwave Anisotropy Probe Observations: Cosmological Interpretation*, *Astrophys. J. Supp.* **180** (Feb., 2009) 330–376, [[0803.0547](#)].
- [51] A. Font-Ribera, P. McDonald, N. Mostek, B. A. Reid, H.-J. Seo and A. Slosar, *DESI and other dark energy experiments in the era of neutrino mass measurements*, *Journal of Cosmology and Astroparticle Physics* **2014** (may, 2014) 023–023.
- [52] D. Spergel, N. Gehrels, C. Baltay, D. Bennett, J. Breckinridge, M. Donahue et al., *Wide-Field Infrared Survey Telescope-Astrophysics Focused Telescope Assets WFIRST-AFTA 2015 Report*, *ArXiv e-prints* (Mar., 2015) , [[1503.03757](#)].